Available online at www.sciencedirect.com
ScienceDirect
Journal of Solid State Chemistry 181 (2008) 90–100
JOURNAL OF SOLID STATE CHEMISTRY
www.elsevier.com/locate/jssc

Perovskite tungsten bronze-type crystals of Li_xWO_3 grown by chemical vapour transport and their characterisation

Claus H. Rüscher[a,*], Kalpana R. Dey[b], Tapas Debnath[a], Ingo Horn[a], Robert Glaum[c], Altaf Hussain[d]

[a]*Institut für Mineralogie und Zentrum für Festkörperchemie und neue Materialien (ZFM), Leibniz Universität Hannover, Welfengarten 1, 30167 Hannover, Germany*
[b]*School of Environmental Science and Management, Independent University, Dhaka 1212, Bangladesh*
[c]*Institut für Anorganische Chemie, Universität Bonn, Gerhard-Domagk-Strasse 1, 53121 Bonn, Germany*
[d]*Department of Chemistry, University of Dhaka, Dhaka 1000, Bangladesh*

Received 16 March 2007; received in revised form 16 October 2007; accepted 30 October 2007
Available online 13 November 2007

Abstract

Crystals of Li_xWO_3 with nominal compositions, $x = 0.1$, 0.25, 0.3, 0.35, 0.4 and 0.45 were grown by chemical vapour transport method using $HgCl_2$ as transporting agent. A complete transport was achieved with a temperature gradient $T_1/T_2 = 800/700\,^{\circ}C$ revealing bluish-black crystals of sizes up to a few 10th of a millimeter. X-ray powder diffraction and infrared (IR) absorption spectra show Perovskite tungsten bronze of cubic symmetry (PTB_c) for $x = 0.45$ and 0.4, mixed phase of PTB_c and Perovskite tungsten bronze of tetragonal symmetry (PTB_t) for $x = 0.35$, 0.3 and 0.25 and of PTB_t and Perovskite tungsten bronze of orthorhombic symmetry (PTB_o) for $x = 0.1$. The structure of PTB_t is explained by the off centring of the W-ions along c and tilting of the WO_6 octahedra around c. Crystal slices of mixed phase (i.e. PTB_c and PTB_t) reveal bright and dark areas on a sub-millimeter scale which are separated by sharp interfaces. Laser ablation inductively coupled plasma optical emission (LA ICP OES) analysis on small spot sizes show the separation into Li contents of $x = 0.18$ (bright areas) and $x = 0.38$ (dark areas) as threshold compositions of PTB_t and PTB_c, respectively. Polarized reflectivity using a microscope technique in the bright area of the crystals indicates strong anisotropic absorption effects with maximum between 1000 and 6000 cm^{-1}, which are related to optical excitations of polarons. Crystals of composition $x = 0.4$ and 0.45 appear optically homogeneous and show an effective "free carrier-type plasma frequency" (w_p) of about 12,900 and 13,700 cm^{-1}, respectively.

Keywords: Perovskite tungsten bronzes; Crystal growth; Polarons; Optical properties

1. Introduction

The Li_xWO_3 Perovskite-type system with variable Li content has a long-standing history of investigations going back to the work of Hägg [1] and Magneli and Blomberg [2]. According to Reau et al. [3] at room temperature a Perovskite tungsten bronze of cubic symmetry (PTB_c) is observed for $0.26 \leqslant x \leqslant 0.5$, of tetragonal symmetry (PTB_t) for $0.095 \leqslant x \leqslant 0.11$, of orthorhombic symmetry (PTB_o) for $0.028 \leqslant x \leqslant 0.032$ and the WO_3 related monoclinic form (PTB_m) for $0.0 \leqslant x \leqslant 0.008$. Reau et al. [3] have obtained their data by X-ray diffraction (XRD) of polycrystalline material synthesized by solid-state reaction at 750 °C of appropriate amounts of Li_2WO_4, WO_3 and WO_2. Similar results have also been reported using in situ X-ray investigations of electrolytic Li/WO_3 cells (4): e.g. the PTB_c and PTB_t are obtained as $0.36 \leqslant x \leqslant 0.5$ (PTB_c), $0.082 \leqslant x \leqslant 0.13$ (PTB_t) and $0.21 \leqslant x \leqslant 0.50$ (PTB_c), $0.078 \leqslant x \leqslant 0.12$ (PTB_t) for charging and discharging, respectively.

The crystal structure of the PTB_c lithium tungsten bronzes has been refined from neutron diffraction data of powder material of $Li_{0.36}WO_3$ [5,6]. The unit cell parameters are twice that of expected in a primitive cubic cell *Pm*-3*m*. The relevant space group becomes *Im*-3 which is

*Corresponding author.
E-mail address: C.Ruescher@mineralogie.unihannover.de (C.H. Rüscher).

0022-4596/$ - see front matter © 2007 Elsevier Inc. All rights reserved.
doi:10.1016/j.jssc.2007.10.033

due to an ordering of Li ions together with a rotation of neighbouring rigid WO_6 in opposite direction of octahedra units. According to this tilt the oxygen coordination of Li tend to become square planar on the partly filled 6*b* (0.5, 0, 0) position with a much shorter Li–O distance of about 217.5 pm instead of 263 pm on the 12-fold coordinated 2*a* sites or 250 pm in the hypothetical untilted phase. Details about the structures of lower x contents lower symmetric phases of Li_xWO_3 could be related to phases of WO_3 that arise in the sequence of its phase transitions [7,8]. According to Locherer et al. [7] the phases of WO_3 changes with increasing temperature from the monoclinic ε-WO_3 (Pc, below 230 K), via triclinic δ-WO_3 (P-1, 230–290 K), monoclinic γ-WO_3 ($P2_1/n$, 290–600 K), orthorhombic β-WO_3 (*Pmnb*, 600–1000 K) to the tetragonal α-forms (α_2 $P4/ncc$ between 1000 and 1170 K and α_1 $P4/nmm$ above 1170 K). Howard et al. [8] reported a modified sequence with *Pbcn* instead of *Pmnb* and with the addition of the monoclinic space group $P2_1/c$ in the sequence of phase transitions between the orthorhombic and tetragonal symmetric phases. The phase transitions are related to the distortion of the octahedra units together with certain tilt of the polyhedra units. The tetragonal form of Li_xWO_3 is related to the α_1 phase of WO_3 [4]. According to the unit cell settings the lattice parameter of PTB_t are related as $a_t = \sqrt{2}a_c$, and $c_t = a_c$, a_c taken as the cubic primitive unit cell. The PTB_o and PTB_m forms of Li_xWO_3 are related by a doubling of the unit cell parameters a, b and c compared to a_c.

There are many recent reports in the field of the Li_xWO_3 Perovskite-type system with a renewed interest in thin film samples, e.g. concerning the electrochromic effect [9–13], (for a review of the literature up to 1995 comparision [14]). On the other hand, single crystal data for this series are rather rare. A single crystal study by Sienko and Truong [15] show the metallic character of conductivity between 100 and 400 K of compositions Li_xWO_3 with x of 0.39, 0.37 and 0.36 that suggests a close similarity to the metallic compositions of Na_xWO_3 and their related free carrier-type optical properties [16]. The question is, however, what happens with further decrease in x concerning the optical properties. Here powder related data and thin film measurements could be misleading. First of all, any anisotropic effect cannot be considered and secondly, there might be no clear separation between the effect of diffusely and regularly reflected light. The investigation of single crystals is highly desirable to obtain a realistic view of the density of states effects from optical data. Therefore, it was our aim to grow suitable size crystals of Li_xWO_3 for studying the optical properties. Here, we report our results of crystal growth in the Li_xWO_3 system by chemical vapour transport and their characterisation in extend our earlier contributions [17,18].

2. Experimental

Crystals were prepared from the appropriate amounts of Li_2WO_4 (Alfa Aesar 99.9%), WO_3 (Alfa Aesar 99.998%) and WO_2 (Alfa Aesar 99.9%) according to the following equation:

$$x/2Li_2WO_4 + (1-x)WO_3 + x/2WO_2 \rightarrow Li_xWO_3, \qquad (1)$$

where $x = 0.1$, 0.25, 0.3, 0.35, 0.4 and 0.45, with total masses of about 110 mg. The reactants were mixed intimately in an agate mortar and taken into clean dried silica tubes (6 mm inner diameter and about 100 mm in length). The silica tubes were then evacuated at room temperature for 2–3 h and sealed. About 3.5 mg of the transporting agent $HgCl_2$ (Alfa Aesar 99.9995%) was added in the silica tubes before evacuation. The reaction tubes were then heated in a double-zone furnace for 5–7 days with a temperature gradient between 700 °C for the sink (T_2) and 800 °C for the source side (T_1). A 100% transport was achieved with this preparation condition, revealing the bluish-black crystals of sizes up to a few 10th of a millimeter. Fig. 1 shows typical scanning electron microscopy (SEM) images (JEOL 820 SEM) and pictures obtained in the optical microscope (reflection mode) of the abraded and polished crystals of selected samples. For nominal composition of $Li_{0.45}WO_3$ and $Li_{0.4}WO_3$ the crystals appear homogeneous in the microscope. Crystals with lower nominal Li content become optically inhomogeneous. For $Li_{0.35}WO_3$ crystals some regularly formed, thin, brighter slabs are observed, which become more distinct for $Li_{0.3}WO_3$. The $Li_{0.1}WO_3$ crystals show plate like shapes and show inhomogeneities on a finer scale.

For the X-ray characterisation a portion of crystals were separated from the batches and carefully ground. A Guinier film method was used (Cu$K\alpha_1$ radiation) with silicon as an internal standard. The 2θ peak positions were measured using a film reader. Indexing and refinement of lattice parameter were carried out using the program package Korgu [19]. For comparison, powder samples were also prepared by using the same reactants with Eq. (1) without transporting agent following the conventional solid-state synthesis method [20]. For these samples powder diffraction data were collected using an automated diffractometer (Phillips PW1800) equipped with Cu$K\alpha$ radiation (graphite monochromator). Structure refinements were performed using the Rietveld software Difrac Plus TOPAS. For the IR investigation 1 mg of the finely ground sample was dispersed into 200 mg KBr and pressed into pellet (13 mm diameter). Measurements were done in the range 370–4000 cm^{-1} (Bruker IFS66v FTIR spectrometer equipped with standard DTGS detector). Spectra are given in absorbance units ($-\lg(I/I_0)$, I_0, I are transmitted intensities through KBr and KBr + sample, respectively).

The optical reflectivity of selected crystals slices as shown in Fig. 1 were measured using an FTIR equipement (Bruker IFS88 with an attached microscope IR scope II). An Al mirror was used for reference measurement. The reflectivity measurements were carried out between 600 and 18,000 cm^{-1} with special detector settings and beam splitters for the ranges 600–4000, 3000–10,000 and 8000–18,000 cm^{-1} providing a sufficient spectral overlap.

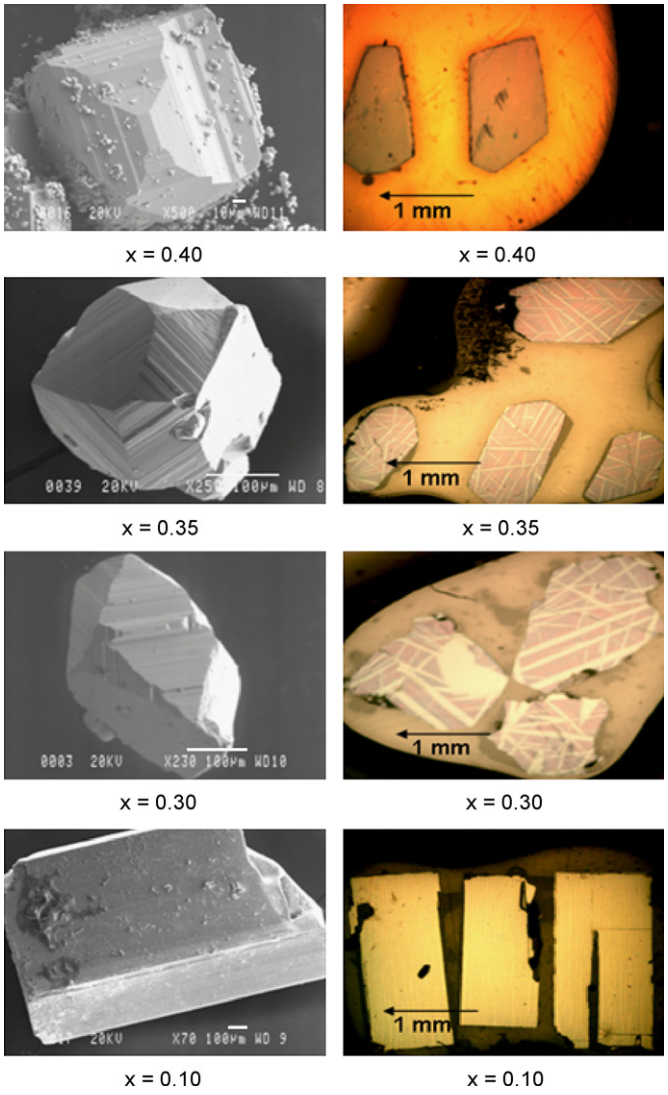

Fig. 1. SEM images (left) and optical microscope images of polished crystals (right) of Li_xWO_3 from batches of nominal compositions as denoted. For $x = 0.35$ and 0.3 crystals bright and dark areas corresponds to boundary compositions of the tetragonal ($x \approx 0.18$) and cubic ($x \approx 0.38$) phase.

A spot size of 80 μm in diameter and polarized light (KRS5 and Glan Thompson polarizer) at nearly normal incidence onto the surfaces were used.

The Li contents with respect to the W signal intensities were measured using laser ablation inductively coupled plasma optical emission (LA ICP OES). The ablated material (aerosol) is flushed by a continuous stream of Ar into the ICP of the spectrometer (Varian Vista Axial ICP OES). For the ablation a home built laser ablation system operating at a wavelength of 196 nm together with a precise *xy* sample stage was used. The spot size of the measurement was about 10 μm diameter. A microscope equipped with a video system enables a direct visualization of the surface and the setting of an accurately rectangular shaped area (e.g. 30 μm × 60 μm) for the integration within dark and bright areas of $x = 0.35$, 0.3 and 0.25 crystals.

3. Results

3.1. X-ray powder results

The phases observed in the X-ray pattern and the refined lattice parameters are given in Table 1. The X-ray powder patterns of $Li_{0.4}WO_3$ and $Li_{0.45}WO_3$ show single-phase PTB_c. Refinements were carried out using space group *Im*-3 as given by Wiseman and Dickens [5]. This setting corresponds to a doubling of unit cell dimension with eight formula units per unit cell compared to a primitive unit cell *Pm*-3*m*. This leads to indexing of all diffraction peaks including the weak ones that could not be indexed using *Pm*-3*m* as shown in Fig. 2a. The lattice parameter values given in Table 1 for the single-phase PTB_c samples are $a_c = a/2$ (*Im*-3) which directly corresponds to W–W distances. The sample $Li_{0.35}WO_3$ shows PTB_c as the major phase along with 2–3 weak lines of PTB_t. For the samples of nominal composition $Li_{0.3}WO_3$ and $Li_{0.25}WO_3$ the contribution of PTB_t systematically increases with respect to the PTB_c content. For the $Li_{0.25}WO_3$ sample about equal portion of PTB_c and PTB_t are observed. Here refinements of the PTB_c contribution were carried out using a primitive setting *Pm*-3*m* since no extra reflection could be resolved from the background. Using only peaks indexed according *Pm*-3*m* in the refinements does not lead to any deviations in the lattice parameter values compared to the refinements with *Im*-3 and $a_c = a/2$.

The samples from the batches of nominal composition $Li_{0.1}WO_3$ show PTB_t with additional three weak lines of PTB_o in the powder diffraction pattern. The lattice parameter of the tetragonal phase of nominal compositions 0.3, 0.25 and 0.1 (Table 1) were refined using space group *P*4/*nmm* suggesting that W is off centred (puckered) along *c* in an untilted WO_3 structure [4–8]. For comparison of the indexing a diffraction pattern of a single phase tetragonal sample as synthesized using the usual solid-state technique is shown in Fig. 2b. It can be seen that all strong peaks can be indexed uniquely. An alternative indexing using space group *P*4/*ncc* is given in brackets. The use of this space group is implied by the observation of the structural modification for WO_3 where the W atoms are off-centred (as in *P*4/*nmm*) and the WO_6 octahedra are additionally tilted around *c* [7,8]. There is a small hint for the presence of the 211 reflection at 2θ of about 40.6° (Fig. 2c inset) which is not allowed in *P*4/*nmm*. The refined pattern and the difference pattern using *P*4/*ncc* is shown in Fig. 2c. The refined structure parameter is given in Table 2 together with the results obtained using alternatively *P*4/*nmm* for comparison. Further arguments for *P*4/*ncc* as the most probable space group for $Li_{0.1}WO_3$ are discussed below. Some small but significant extra peaks are also noted in Fig. 2b that could indicate a more complex structure as discussed below.

3.2. Infrared (IR) absorption spectroscopy

The sample with $x = 0.1$ (Fig. 3) shows strong phonon absorption characteristic with a maximum at 820 cm^{-1}.

Table 1
X-ray results (Guinier method) of crystals of Li_xWO_3 prepared by chemical vapour transport method with a temperature gradient of 100 °C ($T_1 = 800$ °C; $T_2 = 700$ °C); $HgCl_2$ was used as a transporting agent

Nominal composition	Heating period (days)	Phase observed in X-ray for transported crystals	Cell parameter obtained from crystals (Guinier method) (in pm)
$Li_{0.1}WO_3$	7	PTB_t + ■	$a = 520.15(12)$ $c = 384.48(12)$
$Li_{0.25}WO_3$	7	PTB_c + PTB_t	$a = 373.25(13)$ $a = 519.97(9)$ $c = 383.81(11)$
$Li_{0.30}WO_3$	7	PTB_c + PTB_t	$a = 373.22(12)$ $a = 520.29(11)$ $c = 383.79(1)$
$Li_{0.35}WO_3$	7	PTB_c + ●	$a = 373.13(15)$
$Li_{0.40}WO_3$	5	PTB_c	$a = 373.01(7)$
$Li_{0.45}WO_3$	7	PTB_c	$a = 372.04(15)$

● = 2–3 weak extra lines of PTB_t ■ = 3 weak extra lines of PTB_o.

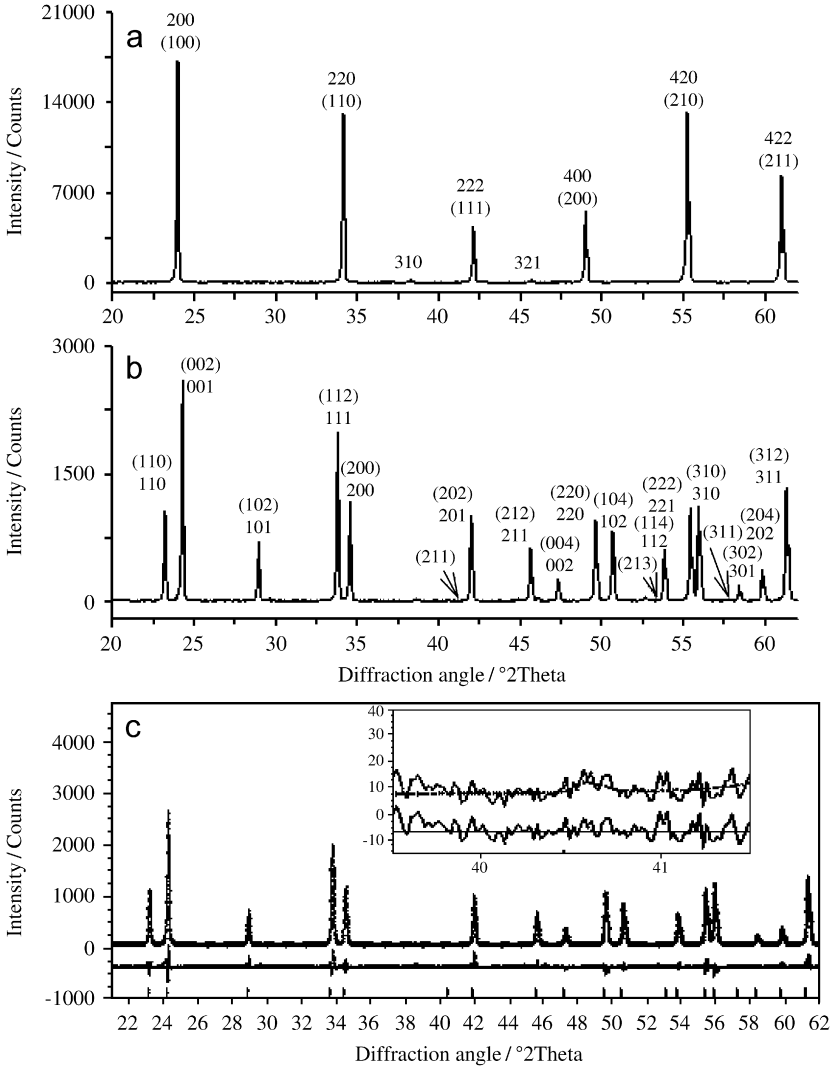

Fig. 2. XRD pattern of cubic (a) and tetragonal (b) Li_xWO_3 with appropriate indexing according to *Im*-3 and *Pm*-3*m* (in bracket) and *P*4/*nmm* and *P*4/*ncc* (in bracket). (c) Result of refinement using *P*4/*ncc* with difference pattern and closer insight for the 2 1 1 peak in the inset.

Table 2
Refined parameters for *P*4/*ncc* (a) and *P*4/*nmm* (b) (Li is not considered)

Atoms	*x*	*y*	*z*
(a) $a = 520.39(1)$ pm, $c = 769.62(2)$ pm			
W	0.25	0.25	0.2846(2)
O1	0.25	0.25	−0.010(3)
O2	0.012(4)	−0.012(4)	0.25
(b) $a = 520.38(1)$ pm, $c = 384.81(1)$ pm			
W	0.25	0.25	0.4310(4)
O1	0.25	0.25	−0.012(5)
O2	0	0	0.5

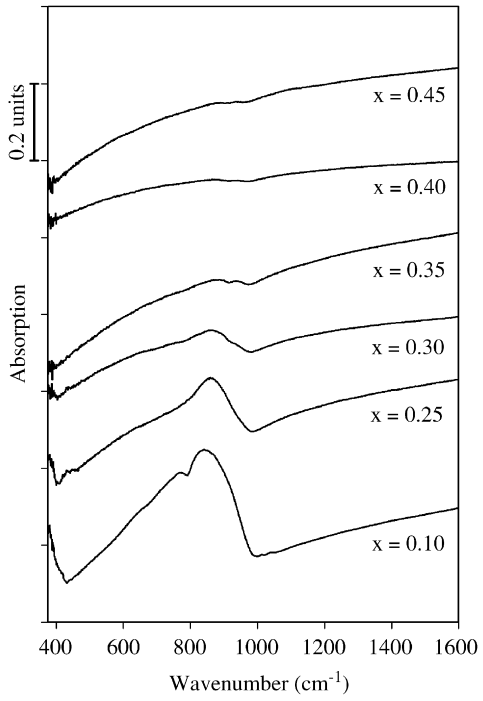

Fig. 3. Infrared absorption of powdered Li_xWO_3 samples (in KBr pressed pellet).

A secondary maximum is seen at 790 cm^{-1} separated by a minimum at about 800 cm^{-1}. The increase in absorption below 420 cm^{-1} indicates another phonon absorption signature, which is outside the measured range and has not been further investigated. For the $x = 0.25$ sample the shape of the spectrum has changed to a single peak maximum at about 830 cm^{-1} and a smaller signature of a double peak around 420 cm^{-1}. It can be concluded that the IR absorption shape observed for the $x = 0.25$ sample typically represents the PTB_t phase. Therefore, the $x = 0.1$ spectra could be more indicative for the PTB_o phase, although noting that this sample shows PTB_t as the major contribution in the XRD pattern. This discrepancy could be explained by an underestimation of short-range order effects in the XRD pattern whereas in IR phonon absorption short-range order effects are seen mainly. Single-phase PTB_c samples ($x = 0.4$, 0.45) only possess just a featureless increase in absorption that increases with increasing wavenumber. Here the phonon contribution is completely negligible compared to the Drude free carrier contribution (no transmissivity, see Fig. 9 and discussion below).

3.3. Polarized optical reflectance

All crystals from the batches of $x = 0.45$ and 0.4 are characterized by their typical reflection spectra shown in Fig. 4a. No variation of the reflection spectra was observed when rotating the crystal in the polarized light. The crystals with nominal composition $x = 0.35$ appear inhomogeneous with thin bright slabs and larger dark areas. The reflectivity of the darker part of the $x = 0.35$ crystals show a similar curve to the $x = 0.4$ crystals. The reflected intensity below 12,000 cm^{-1} appear to be systematically lower compared to the $x = 0.4$ curve. Additionally significant polarisation dependence was also observed as shown in Fig. 4b for the main orientations as denoted by E 0° and E 90°. Similar behaviour is also observed for the dark parts of $Li_{0.25}WO_3$ and $Li_{0.3}WO_3$.

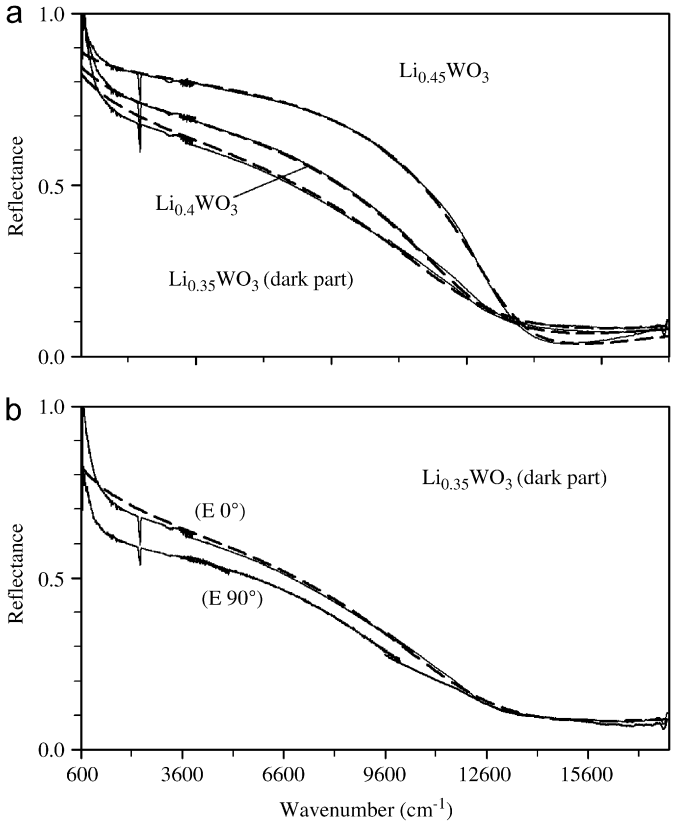

Fig. 4. (a) Measured reflectivity (solid line) and calculated reflectivity (dashed line, Eqs. (2)–(5), for parameter values see Table 3) for $Li_{0.45}WO_3$ and $Li_{0.40}WO_3$ crystals and dark part of $Li_{0.35}WO_3$ crystals (compare Fig. 1). (b) E 0° and E 90° denote spectra obtained for main components parallel to the electric field vector (E) when rotating the crystal slice. Dashed line as in (*a*) for $Li_{0.35}WO_3$.

The curves in Fig. 4a suggest a free carrier-type behaviour and were analysed using the Drude formulas for the dielectric function ($\varepsilon(w)$) according to

$$R(W) = ((n-1)^2 + k^2)/((n+1)^2 + k^2), \quad (2)$$

with

$$n^2 = 0.5[(\varepsilon'^2 + \varepsilon''^2)^{0.5} + \varepsilon'] \text{ and } k^2 = 0.5[(\varepsilon'^2 + \varepsilon''^2)^{0.5} - \varepsilon'], \quad (3)$$

and

$$\varepsilon(w) = \varepsilon' + i\varepsilon'', \quad (4)$$

with

$$\varepsilon' = \varepsilon_\infty(1 - w_p^2/(w^2 + y^2)),\ \varepsilon'' = \varepsilon_\infty y w_p^2/(w(w^2 + y^2)). \quad (5)$$

The wavenumber (w), screened plasma frequency (w_p), and damping constant (y), are given in wavenumber units (cm^{-1}). The "high wavenumber dielectric constant", ε_∞, contains the summed contribution of the valence band electrons. A close approximation of the experimental curves could be achieved with calculated reflectivity curves for parameter values as given in Table 3. A value of 5.5 corresponding to a high frequency reflectivity R_∞ of about 18% was used, which closely agree to the values obtained for the related system of hexagonal tungsten bronzes (HTB) M_xWO_3, M = K, Rb, Cs and $x = 0.2$, 0.25, 0.3, with ε_∞ between 5 and 7 [21]. Owen et al. [16] obtained slightly lower ε_∞ values between 4.4 and 5.4 for PTB_c Na_xWO_3 system with x between 0.86 and 0.52, which systematically increase with decreasing x [note that $\varepsilon_\infty = 1 + \varepsilon_1^b$, with ε_1^b data given by Owen et al. [16]].

For $x = 0.35$ (dark part) and $x = 0.4$ crystals a slightly smaller plasma frequency value of 12,800 cm^{-1} is observed compared to w_p = 13,350 cm^{-1} for the $x = 0.45$ crystals. For a sufficient description of the curves the damping parameter has to be significantly increased for the $x = 0.35$ sample compared to the 0.4 one, where the latter already shows a significantly higher value compared to the $x = 0.45$ crystals. No indication of phonon absorption was observed in the dark area of the crystals. The steeper increase of the experimental curves compared to the calculated one towards lower wavenumber below about 1000 cm^{-1} could indicate a frequency-dependent effect of the free carrier damping. A slight variation in the reflected intensity when rotating the crystal in polarized light was observed for the dark part of the $x = 0.35$ crystal. The lower intensity curve in Fig. 4b cannot be fitted sufficiently well with the Drude model, which could be attributed to some sub-microscopical inhomogeneities, related to Li exsolution effects. The effective damping obtained here for $Li_{0.45}WO_3$ is of the same order as that obtained for HTB phases (2000–4000 cm^{-1}) [21]. Owen et al. [16] observed a systematic increase in the effective damping ($y = 1/t$, t = free carrier relaxation time) with decreasing x for PTB_c Na_xWO_3, i.e. from about 1200 cm^{-1} ($Na_{0.9}WO_3$) to 2500 cm^{-1} ($Na_{0.522}WO_3$). This could imply an overall systematic increase in damping towards lower x values for these systems.

For the bright area of the $x = 0.25$ sample the spectra appear to be strongly anisotropic as shown in Fig. 5. Below 1000 cm^{-1} there are typical phonon peaks. The spectra E 0° show above 1000 cm^{-1} a plateau like reflectivity. Above 4000 cm^{-1} a strong decrease towards a minimum at about 10,000 cm^{-1} is observed. For E 90° there is a similar curve showing; however, a lesser intensity in the plateau between 1000 and 4000 cm^{-1} and a flatter minimum around 10,000 cm^{-1}. The E 90° spectrum could be tentatively described using two oscillator functions with frequencies w_i and oscillator strength F_i for the near IR peak and for phonon signals

$$\varepsilon' = \varepsilon_\infty + \sum_i [F_i w_i^2 (w_i^2 - w^2)]/[(w_i^2 - w^2)^2 + y_i^2 w^2], \quad (6)$$

Table 3
Parameter used with Eqs. (3)–(7): free carrier plasma frequency (w_p), free carrier damping (y), effective high frequency dielectric constant (ε_∞), oscillator eigenfrequencies (w_i), oscillator dampings (y_i), oscillator strengths (F_i)

Nominal composition Li_xWO_3	w_p (cm^{-1})	y (cm^{-1})	ε_∞	w_i (cm^{-1})	y_i (cm^{-1})	F_i
0.45	13,350	3360	5.5			
0.40	12,800	5700	5.5			
0.35	12,800	7400	5.5			
0.25 (E 0°)	3100	800	5	3150	4000	36
				830	50	10
0.25 (E 90°)			5	5200	6300	18
				830	50	7
0.10 (E 90°)			5	5200	4200	2
				830	30	4

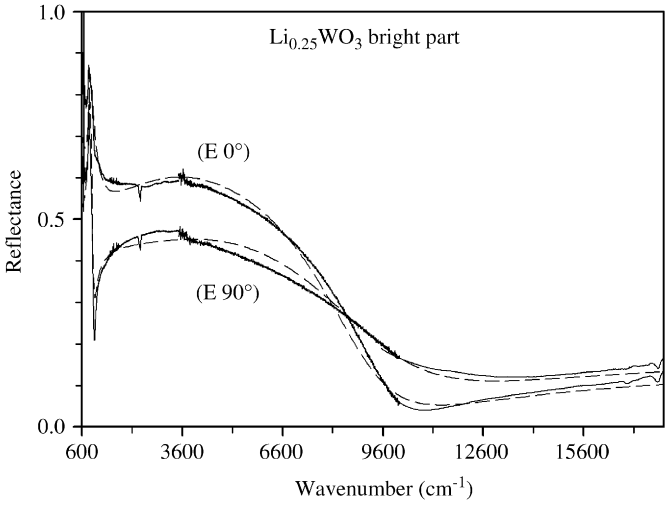

Fig. 5. Measured reflectivity (solid line) and calculated reflectivity (dashed line, Eqs. (2)–(7), for parameter values see Table 3) of bright part of $Li_{0.25}WO_3$ crystals. E 0° and E 90° denote spectra obtained for main components parallel to the electric field vector (E) when rotating the crystal slice.

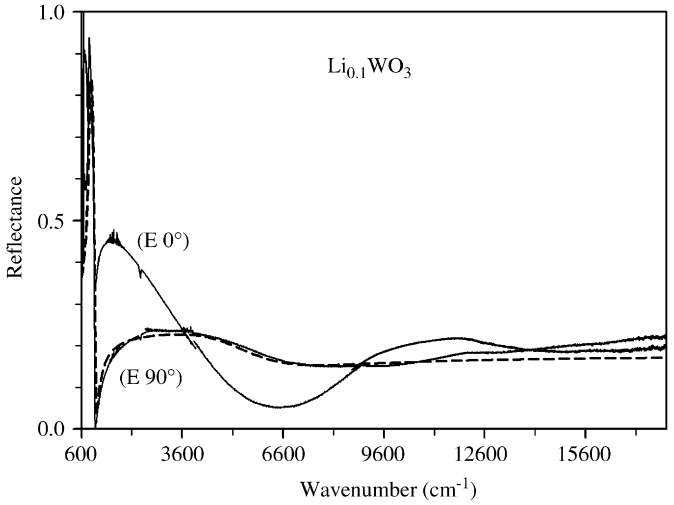

Fig. 6. Measured reflectivity (solid line) of bright part of $Li_{0.1}WO_3$ crystals (Fig. 1). E 0° and E 90° denote spectra obtained for main components parallel to the electric field vector (E) when rotating the crystal slice. Dashed line displays calculated reflectivity (Eqs. (2)–(4), (6), (7); for parameter values see Table 3).

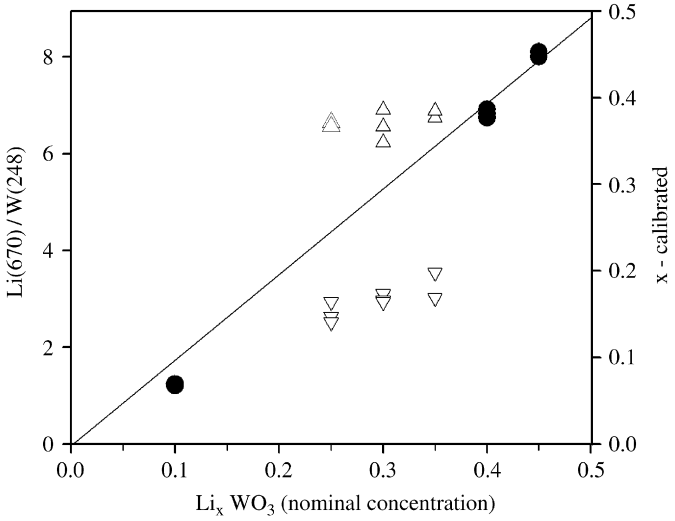

Fig. 7. Results of LA ICP OES analysis for samples of Li_xWO_3 of nominal x. Left scale: Relative signal intensity of Li(670)/W(248). Right scale: Calibrated x scale using $Li_{0.45}WO_3$ and $Li_{0.4}WO_3$ crystals as reference according to the solid line.

$$\varepsilon'' = \sum_t [F_i w_i^2 y_i w]/[(w_i^2 - w^2)^2 + y_i^2 w^2] \quad (7)$$

(w, w_i and y_i are given in wavenumber units). The parameter values are given in Table 3 together with the values used for the E 0° spectrum. For the description of the E 0° spectrum a Drude term (Eq. (5)) was added to describe the strong increase in reflectivity below about 800 cm^{-1}.

The reflectivity spectra of $Li_{0.1}WO_3$ crystals show even a stronger anisotropic reflectivity corresponding to a more significant phonon contribution (Fig. 6). The E 0° spectrum is characterized by a pronounced minimum reflectivity at about 6000 cm^{-1} together with a stronger increase in reflectivity with decreasing wavenumber. Just above 10,000 cm^{-1} there are indications of a further absorption feature. Due to crystal inhomogeneities and possible superimposition effects in the spectra we did not try to fit the E 0° spectrum further. For the E 90° spectrum a good description could be obtained using two oscillator functions with the parameter values as given in Table 3.

3.4. LA ICP OES analysis

The relative signal intensities for Li(670)/W(248) (i.e. Li/W measured by the peak intensity at 670/248 nm, respectively) as obtained for the homogeneous crystals of nominal composition $x = 0.1$, 0.4 and 0.45 are shown by black circles in Fig. 7. The open triangle symbols with top up corresponds to the signal intensities of the dark part of the crystals of nominal compositions $x = 0.25$, 0.3 and 0.35. The open top down triangles is the corresponding values of the bright part. There is some variation in the Li(670)/W(248) intensity as given by the data points for each nominal composition which shows the typical spread of data taken at different measurement points. The crystals of nominal compositions $x = 0.1$, 0.4 and 0.45 show an approximately linear increase in Li content with increasing x. The results of the inhomogeneous crystals are grouped together on a higher and lower level for the dark and bright part of the crystals, respectively. Taking the nominal composition of $Li_{0.45}WO_3$ crystals as an estimate for the compositional calibration (right scale in Fig. 7) implies that the dark and bright part of the crystals indicates the limiting compositions of the miscibility gap between PTB_t and PTB_c at about 0.18 (±0.02) and 0.38 (±0.02) (average values over all measurements).

4. Discussion

4.1. Structural and compositional considerations for PTB_t and PTB_c phases

The lattice parameters (Table 1) as related to the shape of a primitive unit cell $Pm\text{-}3m$ are plotted as a function of nominal Li content in Fig. 8 together with data given by Reau et al. [3] and Dey et al. [20]. Both groups have used solid-state synthesis methods to obtain polycrystalline materials. It can be seen that the general trend in cell parameter variation as well as the absolute values agree closely, suggesting that the crystals grown by chemical vapour transport could well reproduce the properties of the system. The lattice parameter value of the sample $x = 0.4$ is about 1 pm larger compared to the $x = 0.45$ sample. Further decrease in nominal x does not lead to any further increase in a_c and shows that the phase limit has been reached. The saturation in increase in lattice parameter can be related to a limited Li content within PTB_c as obtained by the results of LA ICP OES (Fig. 7). The higher value of the plasma frequency for $Li_{0.45}WO_3$ compared to the

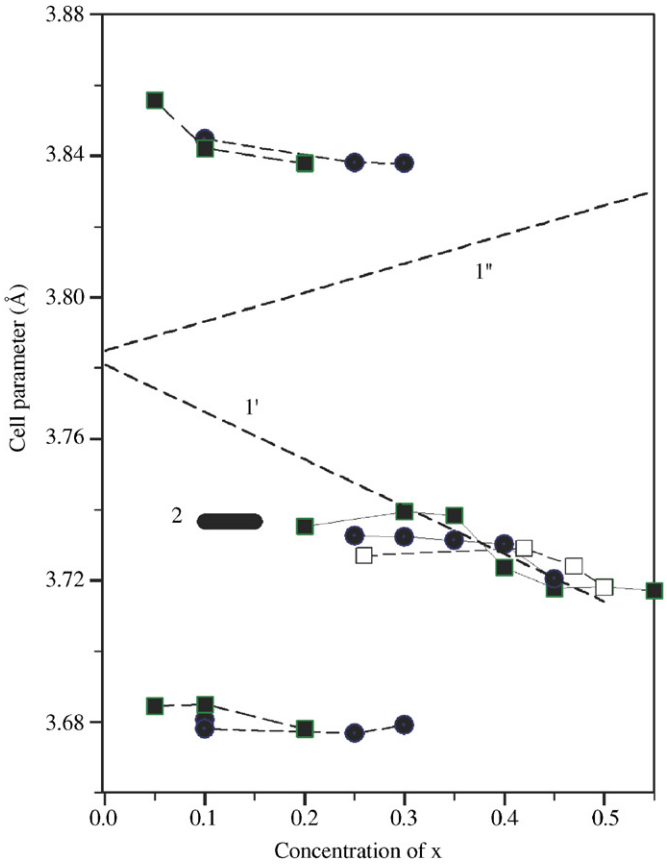

Fig. 8. Comparison of lattice parameter values of Li_xWO_3 system and calculated lines denoted by numbers: (□) = Dey et al. [20], ■ = Reau et al. [3], (●) = this work (Table 1), dashed lines 1′, 1″ = $x \geqslant 0$ extrapolations by Wechter et al. [21] for cubic single phase Li_xWO_3 and Na_xWO_3 compositions, bar (2) = here calculated average value $\langle a_{tc} \rangle$.

$Li_{0.4}WO_3$ crystals (Table 3) can be explained by a higher effective carrier concentration that is related to x, i.e. the increase in Li content seen in Fig. 7. For the dark part of the crystals with $x = 0.35$, 0.3 and 0.25, there is no further decrease in the plasma frequency but an increasing effect of inhomogeneity is probably due to PTB_t contribution distributed on a sub-microscopical scale within the PTB_c matrix.

Wechter et al. [22] proposed an extrapolation from the x dependence of the lattice parameter values from the phase field of cubic compositions Li_xWO_3 with $0.4 < x < 0.5$ and Na_xWO_3 with $0.4 < x < 0.8$ to $x = 0$ according to (in pm)

$$a_c(Li_xWO_3) = -13.4x + 378.1 \text{ and } a_c(Na_xWO_3) = 8.18x + 378.5 \quad (8)$$

(dashed lines 1′ and 1″ in Fig. 8). It can be seen that the $x = 0$ intercepts of both lines 1′ and 1″ closely agree. Therefore, Wechter et al. [22] suggested a value of about 378.5 pm of a theoretical cubic WO_3 lattice at room temperature. Considering the structure determinations based on powder neutron diffraction studies on $La_{0.14}WO_3$, $Na_{0.73}WO_3$, $Na_{0.54}WO_3$ and $Li_{0.36}WO_3$ samples by Wiseman and Dickens [5] a value of about 383.4 pm seems to be more reliable of the aristotype phase of WO_3. By structure refinements a tilted Perovskite structure with space group *Im*-3 was obtained in all cases apart from $La_{0.14}WO_3$ where space group *Pm*-3*m* was used. The tilt is given by oxygen shift from a linear W–O–W bonding which results in an angle (φ) as measured by

$$0.5^*W - W = l^*_{W-O} \cos(\varphi), \quad (9)$$

with a W–W distance of $a_{cp} = 373$ pm and a W–O bond length for $Li_{0.36}WO_3$ of $l_{W-O} = 191.7$ pm the tilt angle becomes 13.6°. For $\varphi = 0°$ this bond length leads to a W–W distance of 383.4 pm which well coincides with the lattice parameter $a_c = 383.4$ pm for the untilted $La_{0.14}WO_3$ [5] with the same W–O bond distance. On the other hand, the $x = 0$ intercept of lines 1′ and 1″ would imply a tilt angle of about 6° considering a W–O bond length of 191.7 pm. Our data for the lattice parameter values of single phase PTB_c compositions indicate a steeper increase for decreasing x values compared to line 1′ and that the $x = 0$ intercept could reach the $\varphi = 0°$ value.

The refined lattice parameter values of the tetragonal contributions PTB_t (Table 1) were recalculated as $a_{tc} = a_t/\sqrt{2}$ and $c_{tc} = c_t$ as measured for better comparison with the lattice parameters of PTB_c as shown in Fig. 8. The bar denoted by number 2 in Fig. 8 corresponds to the average value $(2/3\ a_{tc} + 1/3\ c_{tc}) = \langle a_{tc} \rangle$ which closely agrees to the value a_c of coexisting PTB_c. This shows that the unit volume remains the same for the x dependent transition between PTB_c and PTB_t and that the expansion along c is compensated by a contraction perpendicular to c.

The structure of $Li_{0.095}WO_3$ has been refined by Zhong et al. [4] using space group *P*4/*nmm* which lead to the atomic parameter 0.25, 0.25, 0.432 for W, 0.25, 0.25, 0.932 for O_1 (the two apex oxygen) and 0,0,0.5 for O_2 (the four oxygen in the basal plane) with $a_t = 520.3$ pm and $c_t = 384.4$ pm. According to this the bond length W–O_1 and W–O_2 are 192 and 185 pm, respectively. Our refinement (Table 2) confirm the puckering of W with z coordinate of 0.431 using *P*4/*nmm* and $z = 0.285$ with *P*4/*ncc*. This leads to an absolute value of off centring of about 26.6 pm in both cases. Zhong et al. [4] obtained the same amount of shift of O_1 along z, therefore the W–O_1 distances remain the same. Our data imply that O_1 has a lesser absolute shift, i.e. of about 7.7 pm (*P*4/*ncc*) and 3.8 pm (*P*4/*nmm*). According to this there are alternating shorter and longer W–O_1 distances along the c direction. The same effect is reported for both high temperature tetragonal phases of WO_3 independently by Locherer et al. [7] and Howard et al. [8] (*P*4/*nmm*: $z_W = 0.433$, $z_{O1} = 0.994$, and the same value for *P*4/*ncc*). We observe a significant diffraction intensity at $2\theta = 40.6$ which is indexed as 211 peak in *P*4/*ncc* and not allowed in *P*4/*nmm* (Fig. 2c, inset). Accordingly a tilt of the basal oxygen around the c-axis as described by $a^0a^0c^-$ in the Glazer scheme of tilted octahedra in Perovskites [23] becomes relevant. The same effect has been reported for WO_3 in the tetragonal phase below 950 °C [7,8]. However,

the calculated tilt angle of about 2° seems to be rather small. There are still some weak peaks in the diffraction pattern (Fig. 2b) that indicates that even space group $P4/ncc$ could be inconsistent for a final explanation of the structure of the room temperature form of tetragonal $Li_{0.1}WO_3$.

4.2. Optical properties

Polarized reflectivity of $Li_{0.1}WO_3$ (Fig. 6) and the bright part of the samples Li_xWO_3, $x = 0.25$, 0.3, 0.35 (Fig. 4) reveal typical phonon contributions which are absent in the respective dark part and the $x = 0.4$, 0.45 crystals (Fig. 4) due to the free carrier effect. As shown above the transition from PTB_c to PTB_t is governed by the decrease in Li content with a miscibility gap between 0.18 and 0.38. The reflectivity curves of the PTB_t phases i.e. the bright sections of crystals of nominal composition $x = 0.25$ and 0.3 (Fig. 1), shows remarkable strong anisotropic properties (Fig. 5). The E 0° component may still involve a Drude term with a lower plasma edge $w_p \approx 3100\,cm^{-1}$ (Table 3) whereas such a contribution is absent in the E 90° component in the investigated spectral range. Possibly the E 0° component could be related to polarisation perpendicular to c-axis possessing a higher effective overlap of the electron wavefunction compared to polarisation parallel to c where a more effective localisation of the electron occurs.

The effect of spectral distributions using a Drude term and a combination of Drude and oscillator terms is demonstrated in Fig. 9. The real (ε') and imaginary (ε'') part of the dielectric function (Eqs. (4)–(7)) are shown together with the transmission spectra for $Li_{0.45}WO_3$ and for the PTB_t form of $Li_{0.25}WO_3$ (bright part). The transmission spectra were calculated using

$$T = (1-R)^2(1+k^2/n^2)\exp(4\pi kwd), \quad (10)$$

for a plane parallel plate of thickness $d = 0.1\,\mu m$. The sharp feature around $830\,cm^{-1}$ corresponds to the phonon contribution. Above $8000\,cm^{-1}$ the shape of the curves are similar showing increasing transmissivity values towards the visible range (above $16{,}000\,cm^{-1}$). This absorption effect explains the dark blue colour observed in Li_xWO_3 films and powders. The E 90° component of $Li_{0.18}WO_3$ shows a significant stronger absorption wing ranging into the visible compared to the E 0° component and even compared to the free carrier dominated contribution of $Li_{0.45}WO_3$. The more significant absorption of the E 90° component is related to the highly overdamped Lorentzian together with a higher oscillator frequency compared to the E 0° component used in the description. This indicates a more extended distribution in the density of states for E 90° compared to the E 0° contribution. In a more realistic description of the optical properties one should consider the joint density of states including specific density distribution. This also holds considering polaron formation as a consequence of sufficient strong electron phonon interaction including the effect of disorder [24–27].

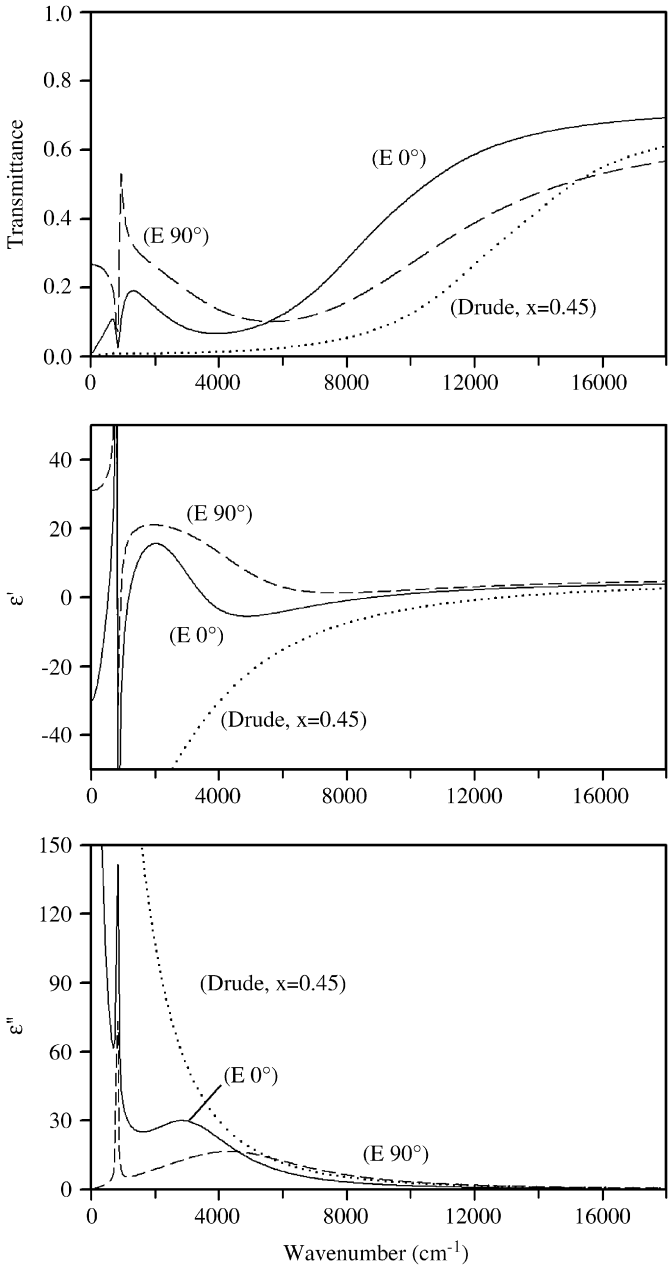

Fig. 9. Calculated transmittance (top), and real (ε', middle) and imaginary (ε'', bottom) part of the dielectric function for $Li_{0.45}WO_3$ (dotted line) and the bright part of $Li_{0.25}WO_3$ for the main components denoted as E 0° (solid line) and E 90° (dashed line) (Eqs. (2)–(8), (10); parameter values given in Table 3).

Considering the formation of small polarons the near IR absorption is dominated by photon assisted hopping of an electron between neighbouring W sites $s1$, $s2$:

$$W^{5+}(s1) + W^{6}(s2) => W^{6+}(s1) + W^{5+}(s2). \quad (11)$$

The small polaron stabilisation energy is estimated as half the energy of the peak maximum of the near IR absorption [28,29] at about ($3150/2\,cm^{-1} \approx$) 0.2 eV and ($5200/2\,cm^{-1} \approx$) 0.32 eV for the coupling parallel and perpendicular to the c-axis. For intermediate sized and larger sized polarons the excitation of internal oscillations

could be considered following a Feynman-polaron model with an oscillator effect for the internal oscillation and a Drude term for the polaron drift contribution [30]. Likalter [31] suggested electron localisation due to Li impurity states in a WO_3 matrix ruling out the polaron effect. We may not rule out that an inhomogeneous Li distribution favours the localisation of electrons. However, due to the strong optical anisotropy we argue that structural details of the WO_3 matrix such as W–O–W bond distances and angles, their dynamics and their flexibility play an important role favouring a strongly anisotropic coupling strength for polaron formation. It may be suggested that the spectra with the stronger phonon contribution is related to a stronger coupling, which occurs parallel to the crystallographic c orientation. Longer W–W distances due to the untilting and, moreover, alternating W–O_1 distances along c as discussed above should lead to an energy gap and insulator like properties for $E//c$. The W–W distances perpendicular to c are smaller suggesting smaller hopping distances and larger overlap of the electron wave functions.

In the Drude description the limiting value of the conductivity at zero frequency is by definition σ_{dc} that is related to the plasma frequency and the damping parameter by

$$\sigma_{dc}(w_p) = w_p^2 \varepsilon_\infty / y. \quad (12)$$

For $Li_{0.45}WO_3$ and $Li_{0.4}WO_3$ $\sigma_{dc}(w_p)$ values read 4761 and 2580 S/cm using w_p, y and ε_∞ from Table 3. These values may be compared with directly measured σ_{dc} data as reported for $Li_{0.36}WO_3$, $Li_{0.37}WO_3$ and $Li_{0.39}WO_3$ single crystals of PTB_c as 6897, 7937 and 11,390 S/cm, respectively [15]. There is a systematic increase in conductivity with increasing Li content for both data sets, i.e. the optical $\sigma_{dc}(w_p)$ values and the directly measured one. The systematically higher σ_{dc} values from direct measurements could be explained by a smaller effective damping of the electrons compared to the damping responsible in the near IR reflectivity. It has been argued earlier for systems like WO_{3-x} [32], $NbO_{2.5-x}$ [33], and ternary Nb–W oxides [34], that an insulator to metal transition occurs at a so called polaron saturation concentration above which polarons and free carriers coexists. At the transition point the optical properties change to Drude-type behaviour in these systems [35,36]. A similar change in the optical properties is observed for the Li_xWO_3 system for the cross over from PTB_t to PTB_c related to x. A more general question is, however, if there is a mixing of polarons and free electron charge carriers. It could be more suitable to consider here just a gas of polarons for PTB_c of Li_xWO_3 to explain the optical properties.

5. Conclusion

Suitable crystals in the system Li_xWO_3 were grown by chemical vapour transport method for investigating their chemical composition and optical properties using microscope techniques. Inhomogeneties of crystals of nominal composition $x = 0.35$, 0.3, 0.25 were used to determine the threshold compositions of the miscibility gap between PTB_c and PTB_t. Lattice parameter values of powder-related X-ray data could be explained by a decrease in WO_6 octahedral tilt with decreasing x in the PTB_c phase region. LA ICP OES data as well as the plasma frequencies indicate a decrease in Li content with decreasing x, too. For PTB_t the puckering effect, i.e. the off centring of W along c and tilting of WO_6 octahedra around the c-axis occurs, which is consistent with the XRD pattern indexing with the higher symmetry space group $P4/ncc$ instead of $P4/nmm$.

The bright part of the crystals of Li_xWO_3 with $x = 0.25$, 0.3, 0.35 i.e. $Li_{0.18}WO_3$ as the upper concentration limit of the PTB_t phase field, show strong anisotropic effects and phonon contributions. For E perpendicular to c a tilt effect of the WO_6 octahedral units (tilt axis parallel to c) is present. For E parallel to c the lack of tilting should lead to a wider conduction bandwidth. However, it is concluded that insulator like properties are observed for $E//c$ due to the effect of long/short W–O–W–O bond alternation.

Acknowledgments

This work has been supported in part by the "Alexander von Humboldt Stiftung" under collaborative research program (V-FOKOOP/DEU/1062067/Hussain) and DFG (RU764/4-1). K.R. Dey is grateful for the "Lichtenberg Stipendium" of the "Land Niedersachsen" (Germany) for the support of her Ph.D. work and to Prof. Binnewies (ACI, Leibniz University Hannover) for the support with crystal growth facilities. Finally, the authors are thankful to three unknown referees and to the editor for helpful comments.

References

[1] G. Hägg, Z. Phys. Chem. B 29 (1935) 192.
[2] A. Magneli, B. Blomberg, Acta Chem. Scand. 5 (1951) 372.
[3] J.M. Reau, C. Fouassier, G. Leflem, J.Y. Barraval, J.P. Doumere, P. Hagenmuller, Revue Chimie Miner. t7 (1970) 975.
[4] Q. Zhong, J.R. Dahn, K. Colbow, Phys. Rev. B 46 (1992) 2554.
[5] P.J. Wiseman, P.G. Dickens, J. Solid State Chem. 17 (1976) 91.
[6] R.J. Cava, A. Santoro, D.W. Murphy, S.M. Zahurak, R.S. Roth, J. Solid State Chem. 50 (1983) 121.
[7] K.R. Locherer, I.P. Swainson, E.K.H. Salje, J. Phys.: Condens. Matter 11 (1999) 6737.
[8] C.J. Howard, V. Luca, K.S. Knight, J. Phys.: Condens. Matter 14 (2002) 377.
[9] P.R. Bueno, R.C. Faria, C.O. Avellaneda, E.R. Leite, L.O.S. Bulhoes, Solid State Ionics 158 (2003) 415.
[10] S.H. Lee, H.M. Cheong, C.E. Tracy, A. Mascarenhas, A.W. Czanderna, S.K. Deb, Appl. Phys. Lett. 75 (1999) 1541.
[11] C.O. Avellaneda, P.R. Bueno, L.O.S. Bulhoes, J. Non-Cryst. Solids 290 (2001) 115.
[12] C.O. Avellaneda, L.O.S. Bulhoes, J. Solid State Electrochem. 7 (2003) 183.
[13] C.O. Avellaneda, L.O.S. Bulhoes, Solid State Ionics 165 (2003) 59.

[14] C.G. Granqvist, Handbook of Inorganic Electrochromic Materials, Elsevier, Amsterdam, 1995.
[15] M.J. Sienko, T.B.N. Truong, J. Am. Chem. Soc. 83 (1961) 3939.
[16] J.F. Owen, K.J. Teegarden, Phys. Rev. B 18 (1978) 3827.
[17] K.R. Dey, A. Hussain, C.H. Rüscher, in: Asian Crystallographic Association (AsCA'04) Conference. Hong Kong, 27–30 June 2004, p. PO182.
[18] C.H. Rüscher, K.R. Dey, I. Horn, A. Hussain, Z. Krist. 22 (Suppl) (2005) 100.
[19] Korgu, Lyrt, Asin program package, MS DOS version of VAX code from M. Möller, Ph.D. Thesis, University of Dortmund, 1983.
[20] K.R. Dey, C.H. Rüscher, Th.M. Gesing, A. Hussain, Mater. Res. Bull. 42 (2007) 591.
[21] A. Hussain, R. Gruehn, C.H. Ruscher, J. Alloys Compds. 246 (1997) 51.
[22] M.A. Wechter, H.R. Shanks, A.F. Voigt, Inorg. Chem. 7 (1968) 845.
[23] A.M. Glazer, Acta Crystallogr. A 31 (1975) 756.
[24] H. Böttger, V.V. Bryksin, Hopping Conduction in Solids, VCH, 1985.
[25] C.H. Rüscher, M. Götte, B. Schmidt, C. Quittmann, G. Güntherodt, Physica C 204 (1992) 30.
[26] C.H. Ruscher, M. Götte, Solid State Commun. 85 (1993) 393.
[27] C.H. Rüscher, in: E.K.H. Salje, A.S. Alexandrov, W.Y. Liang (Eds.), Polarons and Bipolarons in High T_c Superconductors and Related Materials, Cambridge University Press, Cambridge, 1995, p. 206.
[28] I.G. Austin, N.F. Mott, Adv. Phys. 18 (1969) 41.
[29] H.G. Reik, in: J.T. Devreese (Ed.), Polarons in Ionic Crystals and Polar Semiconductors, North-Holland Publ. Comp., Amsterdam, 1971, p. 679.
[30] R. Evrard, in: J.T. Devreese (Ed.), Polarons in Ionic Crystals and Polar Semiconductors, North-Holland Publ. Comp., Amsterdam, 1971, p. 29.
[31] A.A. Likalter, J. Phys.: Condens. Matter 315 (2002) 252.
[32] E. Salje, B. Güttler, Philos. Magn. B 50 (1984) 607.
[33] C. Rüscher, E. Salje, A. Hussain, J. Phys. C: Solid State Phys. 21 (1988) 3737.
[34] C. Rüscher, E. Salje, A. Hussain, J. Phys. C: Solid State Phys. 21 (1988) 4465.
[35] C.H. Rüscher, Physica C 200 (1992) 129.
[36] C.H. Rüscher, M. Zimmermann, M. Gotte, Z. Naturforsch. 48a (1993) 443.